INTERNATIONAL Agrophysics

www.international-agrophysics.org

Int. Agrophys., 2026, 40, 67-79 doi: 10.31545/intagr/211392

Early detection of wheat germination using image analysis with a preliminary exploration of its onset prediction based on imbibition development

Jakub Lev[®]*, Jiří Blahovec[®]

Department of Mathematics and Physics, Czech University of Life Sciences Prague, Kamýcká, 165 00, Praha – Suchdol, Czech Republic

Received June 6, 2025; accepted September 26, 2025

Abstract. Research on imbibition and germination is currently a topic of great interest among researchers. One cost-effective yet efficient approach to monitoring imbibition and germination is the use of image analysis. In this study, a total of 404 winter wheat grains (Triticum aestivum L.) of four different varieties were examined. Image data were captured using a high-resolution camera controlled by a computer. The grains were analysed for their size and shape described by the image moment $(\eta_{2,0})$. Fourteen parameters were proposed, which were subsequently used to characterise the development of the grains during imbibition and germination. The progression of the image moment indicated that wheat grain imbibition and germination could easily be divided into three distinct phases: in the first, hydration occurs predominantly in the embryo, followed by the endosperm in the second. The third phase consists of the germination itself. The minimum of the image moment course marks the onset of germination, occurring at a stage when radicle development is still imperceptible to human evaluators. Germination identified in this manner can thus be partially predicted from the aforementioned parameters. The linear model yielded a coefficient of determination of 0.5017.

K e y w o r d s: image moments, linear model, radicle detection, cost-effective

1. INTRODUCTION

Germination is one of the primary events in the growth of wheat and all plants in general. Consequently, many researchers have studied the details of this process and sought to understand it (Bewley 1997; Kornarzyński *et al.*,

2018; Diaz-Mendoza et al., 2019). One of the key factors influencing germination is water absorption by the seed (Al-Karaki 1998; Gómez-Maqueo et al., 2020). This water enables the initiation of essential physiological processes that ultimately culminate in sprout formation (Abenavoli et al., 2006). Many researchers have recently focused on this initial stage of seed germination, known as imbibition (Louf et al., 2018; Visscher et al., 2020; Zhao et al., 2020). Imbibition and its dynamics are also studied in connection with the issue of preharvest sprouting and seed priming (Mares and Mrva, 2014; Tanwar et al., 2023). Imbibition is commonly monitored through repeated seed weighing (Abenavoli et al., 2006; Dell'Aquila, 2009). This is a labourintensive procedure that can be partially replaced or complemented by other methods, such as near-infrared hyperspectral imaging (Manley et al., 2011; Lancelot et al., 2017), moistening seeds in dye solutions (Salanenka and Taylor, 2011; Lev et al., 2019), or electromagnetic radiation exposure, that is, irradiation with neutron beams or X-rays (Nakanishi and Matsubayashi, 1997; Nielsen et al., 2017).

An established method for monitoring water content in seeds is nuclear magnetic resonance (NMR) (Gruwel *et al.*, 2001; Kikuchi *et al.*, 2006; Ghosh *et al.*, 2007; Borisjuk *et al.*, 2012). This method also enables the tracking of water penetration into different parts of the seed (Munz *et al.*,

© 2026 Institute of Agrophysics, Polish Academy of Sciences



2017). NMR can be conducted non-invasively in live seeds, minimising the impact on their natural development (Van and Van Duynhoven, 2013).

The process of wheat grain hydration was described in detail using NMR by Rathjen *et al.* (2009): from the first minute it is moistened, the grain absorbs water very rapidly, with water initially entering the bilayer between the grain coat and the pericarp and reaching the embryo through the micropyle. In the following 4-6 h, the entire embryo is hydrated, and water enters the scutellum, aleurone layer, and endosperm. Other studies focus on water movement and distribution during moistening in other plants, such as tobacco (Manz *et al.*, 2005) or rapeseed (Munz *et al.*, 2017).

As previously mentioned, the presence of water in certain parts of the grain is a necessary condition for initiating physiological processes associated with germination. Therefore, real-time tracking of water movement within the grain is highly valuable for studying these processes (Gómez-Maqueo et al., 2020). Image analysis can be used for this purpose (Wiesnerova and Wiesner, 2008; Dell'Aquila, 2009; Nehoshtan et al., 2021). It is primarily employed for the automatic detection of visible germination (Ducournau et al., 2004; Awty-Carroll et al., 2018) or for seed sorting and phenotypic analysis (Mebatsion et al., 2012; Loddo et al., 2021). Several automated systems have been developed for this purpose: GERMINATOR (Joosen et al., 2010), SmartGrain (Tanabata et al., 2012), PhenoSEED (Halcro et al., 2020), SeedGerm (Colmer et al., 2020), and SeedExtractor (Zhu et al., 2021). These systems evaluate seeds based on size, shape, and colour.

Germination is often determined based on changes in certain parameters resulting from the development of the sprout. For example, Ducournau et al. (2004) compared the seed's outline to its initial outline at the start of monitoring. Germination was detected when a significant change occurred. Awty-Carroll et al. (2018) used the k-NN method to detect germination. This method worked relatively well, although the goal was to detect advanced germination, and the training data already included data with developed sprouts. The GERMINATOR system (Joosen et al., 2010) detected germination by comparing the position of the seed's centroid and its area, identified using two different colour thresholds. This method leveraged the fact that the sprout and the seed have different colours; thus, the seed was detected with the first threshold, while the second threshold detected both the sprout and the seed.

As yet, only few studies utilise image analysis to monitor imbibition. Dell'Aquila (2004) used image analysis to examine temporal changes in the area size and roundness factor of broccoli seeds. While the roundness factor could be used to detect the growing sprout, the increasing area of the seeds during moistening significantly correlated with weight gain. Additionally, Wiwart *et al.* (2006) found a significant correlation between seed weight and certain shape parameters when studying the imbibition of triticale

seeds. Miller *et al.* (2018) investigated the imbibition of corn using two methods. The first was based on measuring the force induced by swelling, while the second estimated size changes in seeds using image analysis. The authors noted that imbibition was more significantly influenced by its genotype than by the environment in which it was produced and stored. We discussed the monitoring of winter wheat imbibition using image analysis in our previous article (Lev and Blahovec, 2017). By capturing subtle changes in the area and shape of the seeds, it was possible to detect water entering the embryo through the micropyle and the subsequent swelling of the embryo. These events were distinguishable.

This study addresses the possibilities of using image analysis for the precise monitoring of wheat grains throughout the entire process of imbibition and the onset of radicle development. The approach monitors selected parameters of imbibition, its dynamics, and the potential for earlier detection of germination, including the connection between imbibition and germination.

2. MATERIALS AND METHODS

The device for monitoring the wheat grains was placed in a laboratory box that maintained an approximately stable temperature during measurements. The device consists of a camera mounted on a stand (Canon 450D with Canon EFS 18-55 mm lens), an LED lighting panel (neutral white, 6000 K), and a glass container for the monitored cereal grains. The device is illustrated and described in detail in Fig. 1. The control of both the camera and the LED panel was managed by a computer. For the camera, the software DSLR Remote for Windows version 2.7.2 (Breeze Systems, UK) was used, while a custom control program was used

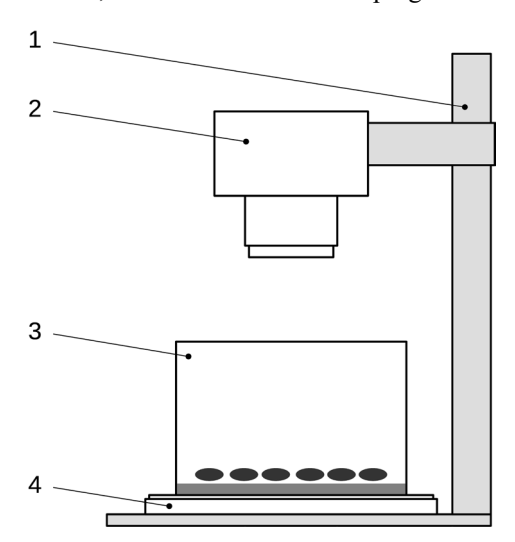


Fig. 1. Diagram of the laboratory setup for photographing samples. The entire assembly is placed in a dark box. The system is fully automated, with the lights and camera controlled from a computer: 1-stand, 2-camera, 3-glass vessel with monitored grains, 4-illumination LED panel.

for the LED panel. The lighting panel was automatically turned on 3 s before each image capture and was turned off immediately after the image was taken (for most of the test, the wheat grains were kept in the dark). The photographs were stored on the computer hard disk in RAW format immediately after being taken. The photographs were taken at a resolution of 4290×2856 pixels.

Measurements were conducted at the beginning of 2017 (from January 4 to March 6). The winter wheat grains (*Triticum aestivum* L.) were harvested in 2016 and supplied by Selgen Plc Company. The initial moisture content ranged between 7% and 9% (ASABE Standard S358.2, 2006). Very small and large grains were excluded from the samples using an air stream (Kroulík *et al.*, 2016). A pneumatic separator K-293 (VEB Kombinat Fortschritt; Anlagenbau Petkus, Wutha, Germany) was used for this purpose. The air velocities for grain separation were set to 9.5 and 11.7 m s⁻¹. Four varieties were tested: Tosca, Vanesa, Turandot, and Steffi; the weight per 1000 seeds (after excluding small and large grains) varied slightly at 46.4, 52.9, 52.3, and 50.5 g, respectively. The temperature in the laboratory box ranged from 20 to 21.5°C.

Agar 0.8 was used as the medium for germinating the tested seeds. The optical properties of agar allow for a significant optical contrast between the tested grains and the background. The container with the agar and the observed grains was covered with a thin glass plate (3 mm thick) to reduce agar dehydration during the experiment. The grains were evenly placed on the agar, always with the crease facing downwards. The area occupied by the grains was kept uniform so that the lens covered it entirely. Each sample contained 24 grains, and 4 samples were tested for each variety (a total of 96 grains per variety). An exception occurred in the first tested variety, Tosca, where the sample size was initially 20 grains and later 24. The number of samples for this variety was 5 (for a total of 116 grains). The interval between photographs was always 5 min. Each experiment was concluded after all seeds in the container had germinated or after a maximum of 3 days of observation. Additionally, a rectangular PVC plate was placed in the container as a scale. This scale was used to determine the pixel size (the imaged area corresponding to one pixel, with an approximate size of 14 µm) in the subsequent image analysis of individual grains. The distribution of the grains in the container is visible in Fig. 2.

The initial analysis of the images was conducted using the Python programming language (version 3.4, https://www.python.org) and supporting libraries: NumPy 1.14.1 and OpenCV 3.4.0. The primary objective was to determine the monitored parameters of individual grains in each image. The first step in image processing consisted in converting the RGB image to greyscale. The blue channel was utilised for this purpose, as it provided the highest contrast between the grains and the background. The image was subsequently binarised using a threshold value of 100

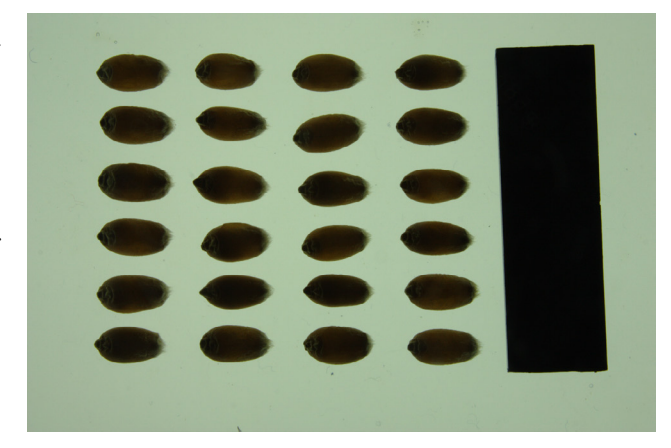


Fig. 2. Photograph of the grains at the beginning of the experiment. The image shows 24 grains of the Turandot variety. A scale measuring 9.8 x 32.5 mm is positioned on the right.

(8-bit colour depth). The threshold was selected based on an analysis of the image histogram. As the lighting conditions were kept consistent throughout all measurements, it was not necessary to adjust the threshold value. The next step involved applying an erosion-dilation filter (Gonzalez and Woods, 2002) to reduce noise. Each tested grain's image was oriented so that the main axis of the displayed grain was parallel to the x-axis of the image. Central image moments (Gonzalez and Woods, 2002) were used to find the main axes of the grains, which are formally defined by the expression:

$$\mu_{p,q} = \sum_{x} \sum_{y} (x - x_c)^p (y - y_c)^q f(x, y), \tag{1}$$

where: p and q are natural numbers, x_c and y_c are the coordinates of the centroid of the displayed grain, and f(x,y) represents the individual pixels of the digital image of the grain. The angle of rotation of the grain's x-axis, denoted by θ , is given by the expression:

$$\theta = \frac{1}{2} \arctan\left(\frac{2\mu_{1,1}}{\mu_{2,0} - \mu_{0,2}}\right),\tag{2}$$

where: $\mu_{1,1}$, $\mu_{2,0}$, and $\mu_{0,2}$ are the central moments defined in Eq. (1). For each grain, the following parameters were calculated: grain area, its length, width, and its normalised central moment of area $\eta_{2,0}$. These parameters were then used for further analysis. The length and width were determined using the boundingRect() function from the OpenCV library. The moment $\eta_{2,0}$ was calculated on the already rotated grain contour and is defined by the following expression:

$$\eta_{2,0} = \frac{\mu_{2,0}}{\mu_{0,0}^2},\tag{3}$$

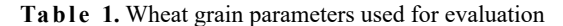
where: $\mu_{0,0}$ is the image moment corresponding to the area of the grain. After the preliminary analysis, it was found that the time course of $\eta_{2,0}$, as well as the course of the length-to-width ratio (l/w), contains two extrema. The first is a maximum at time t_1 , and the second is a minimum at

time t_2 . Between these points, at time t_{infl} , lies an inflection point. The curve representing the course of η_2 ,0, along with the marked times, is shown in Fig. 3a. The detection of points t_1 and t_2 was performed by fitting a polynomial to the region where an extremum was expected and then identifying the maximum or minimum on the fitted curve. To detect the inflection point, the data from t_1 to t_2 were iteratively fitted with a straight line (with a segment length of 10 h). The inflection point corresponded to the centre of the interval where the absolute magnitude of the slope was the highest.

In Figure 3b, the curve represents the course of grain area increment during hydration. In the interval from t_1 to t_2 , hydration primarily affects the endosperm, so the development of the area can be described by a relatively simple function (Rathjen *et al.*, 2009):

$$a_t = \frac{c_1 \tau}{c_2 + \tau} \,, \tag{4}$$

where: a_t is the increase in the grain area from time t_1 , τ is the time elapsed since t_1 , and C_1 and C_2 are constants of the equation. The constant C_1 corresponds to the limit value of a_t at infinity, representing the theoretical maximum increase in grain area due to swelling. C_2 is the time constant, which indicates the time τ at which the increase a_t reaches half of C_1 . Eq. (4) was used to approximate the data obtained for all examined grains. The average value of the coefficient of determination r^2 was 0.996, with a minimum value of 0.936. These values indicate that the equation describes the area development between times t_1 and t_2 with a high level of precision.



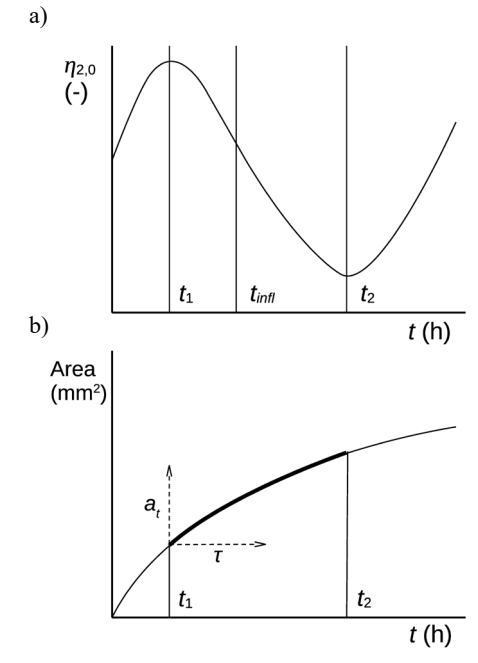


Fig. 3. a) A curve representing the typical course of $\eta_{2,0}$ with the marked points t_1 , t_2 , and tinfl. b) Typical course of grain area increment during hydration. The region between t_1 and t_2 is highlighted and was fitted using Eq. (4).

To describe and gain a deeper understanding of the details of germination, we introduced several additional parameters, which are listed in Table 1. In addition to the time points $(t_1, t_2, \text{ and } t_{infl})$, the initial values of the area and the image moment $\eta_{2,0}$ are provided, along with other parameters that express the development of grains during imbibition and germination.

Parameter	Parameter description and unit
t_1	Time of $\eta_{2,0}$ maximum (h)
t_2	Time of $\eta_{2,0}$ minimum, the onset of germination (h)
t_{infl}	The moment of the inflection point on $\eta_{2,0}$ (between t_1 a t_2) (h)
a_0	Initial grain area (mm²)
η_0	Initial moment $\eta_{2,0}$ (-)
ΔA_1	Relative area change in t_1 (-), $\Delta A_1 = [a(t_1)-a_0]/a_0$ *
$\Delta \eta_1$	Change of $\eta_{2,0}$ in t_1 (-), $\Delta \eta_1 = \eta_{2,0}(t_1) - \eta_0$ *
ΔA_{12}	Relative area change between t_1 and t_2 (-), $\Delta A_{12} = [a(t_2)-a(t_1)]/a_0$ *
$\Delta\eta_{12}$	Change of $\eta_{2,0}$ between t_1 and t_2 (-), $\Delta \eta_{12} = \eta_{2,0}(t_2) - \eta_{2,0}(t_1)$ *
AR_1	Area change rate to t_1 (h ⁻¹), $AR_1 = \Delta A_1/t_1$
C_{1n}	Normalised C_1 (-), $C_{1n} = C_1/a_0$
C_{ratio}	$C_{ratio} = C_{1n}/[2 \ C_2]$
$\eta_{ m S}$	$\eta_{2,0}$ slope in t_{infl} (h ⁻¹)
l_S	Radicle growth rate in the interval between t_2 and $t_2 + 10$ h (mm h ⁻¹)

^{*}a(t) and $\eta_{2,0}(t)$ represent grain area or grain image moment at time t (t_1 or t_2).

The parameters listed in Table 1 were calculated for all analysed grains. The parameter determination was performed later than the initial image analysis; therefore, newer versions of tools were used, including Python (version 3.10) and NumPy (version 2.1.2). Additionally, the libraries SciPy (version 1.14), Matplotlib (version 3.9.2), and the statistical program R (https://www.r-project.org, version 3.0.2) were utilised. For certain analyses (principal component analysis and multiple linear regression), the data were normalised according to the equation:

$$Z = \frac{x - u}{\sigma} \,, \tag{5}$$

where: z represents the normalised data, x denotes the original data, μ is their mean value, and σ is the corresponding standard deviation. For the principal component analysis, the Scikit-learn library (https://scikit-learn.org, version 1.7) was used, and the computation itself was programmed in Python. Prior to the actual analysis, correlations between the examined parameters were calculated.

3. RESULTS AND DISCUSSION

The development of the area, length, and width of the grains over time exhibits a similar pattern, with the highest growth rate occurring at the beginning of the test. Subsequently, the growth rates of both dimensions decrease until the onset of germination. Significant differences are observed in the growth patterns of length and width: at the beginning of the experiment, the length of the grain increases faster than its width; however, at time t_1 , this trend reverses, and the width of the seed continues to increase faster than its length, resulting in a decrease in the lengthto-width ratio (Fig. 4c). This trend ends at time t_2 in relation to the observed growth of the radicle; at this time, the trend reverses again, and the length increases significantly more than the width, causing the length-to-width ratio to rise. The temporal progression of the length-to-width ratio of the seed throughout the test lacks "smoothness" (Fig. 4c); therefore, further analysis uses an area-based description of the observed phenomena using the central image moments $\eta_{2,0}$ Eq. (3), which describe the development of the grain in a manner similar to the ratio of its length and width (Fig. 4a).

The parameter $\eta_{2,0}$, similar to the ratio l/w, exhibited two extremes during the imbibition process (Fig. 4a, c). The first is a maximum at the time marked t_1 , and the second is a minimum at the time t_2 . The development of the grain can be divided into three phases: the first phase ends at time t_1 , which in this example occurs around 4 h. It is known (Rathjen *et al.*, 2009) that, during this phase, water first enters the grain through the micropyle and hydrates its embryo. The embryo is relatively small, and its swelling is manifested only by a slight yet reliably detected elongation of the grain and an increase in $\eta_{2,0}$.

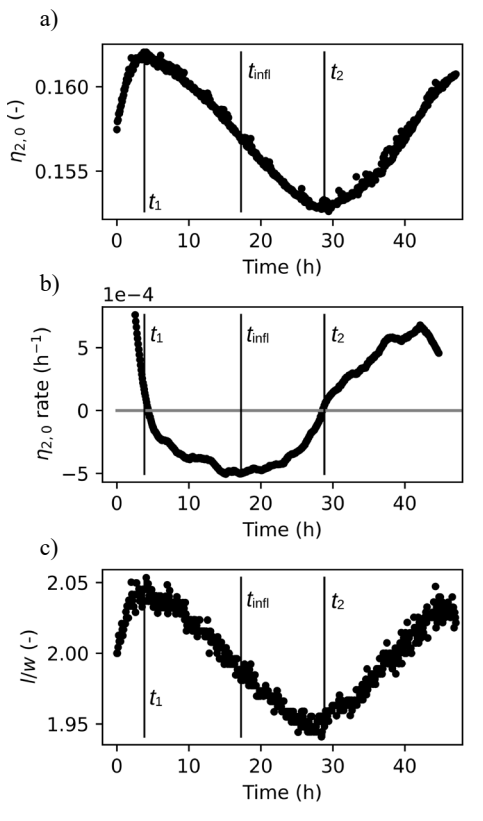


Fig. 4. Example of the development of quantities characterising changes in the grain shape during germination: the central image moment of the grain $\eta_{2,0}$ (a), the derivative of the central image moment of the grain $\eta_{2,0}$ with respect to time (b), and the ratio of length (*l*) to width (*w*) of the grain (c). The data presented are for the Turandot variety (grain no. 51). In all graphs, the times t_1 , t_2 , and t_{infl} (inflexion point on $\eta_{2,0}$) are marked. The derivative in (c) was determined by successively fitting a line to the data over 5-hour intervals.

The development pattern of the image moment $\eta_{2,0}$ corresponds to the gradual hydration of the embryo and the endosperm. The phases separated by times t_1 and t_2 may resemble the classical three-stage theoretical germination model (Bewley, 1997), where the first stage involves rapid water uptake, the second shows a pause in uptake, and the third stage involves the germination itself, marked by renewed water uptake. For instance, Moret-Fernández et al. (2024) modelled the imbibition process by treating the grain as a homogeneous porous material. However, for the wheat grains examined in our study, it appears more appropriate to describe the embryo and the remainder of the grain (endosperm) separately. In the case of the embryo, the standard three-stage model may align well. The embryo becomes fully hydrated within several hours, and additional water uptake does not occur until germination begins. The t_1 point could likely serve as an indicator that the embryo has reached saturation. In contrast, the endosperm absorbs

water slowly throughout the entire germination process, showing no clear distinction between the first and second phases (Kornarzyński *et al.*, 2002).

If the grain does not germinate, the decrease in $\eta_{2,0}$ over time weakens until it stabilises at a constant value (Lev *et al.*, 2017). However, if the radicle begins to develop, the grain elongates, and $\eta_{2,0}$ starts to rise again at time t_2 . In this phase, hydration plays a dominant role in the development of the embryo. Besides t_1 and t_2 , the graph in Fig. 4 also marks the time t_{inft} . At this time, an inflection point is detected, representing the state with the fastest decrease in $\eta_{2,0}$ indicating the onset of a gradual slowdown in the decrease of the $\eta_{2,0}$ parameter.

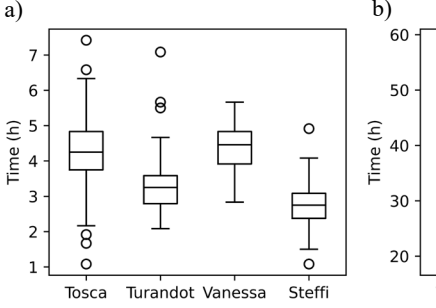
The times t_1 and t_2 are displayed for each variety in Fig. 5 and can be seen to differ from each other. In the case of t_1 (Fig. 5a), statistically significant differences were found among all varieties except between Tosca and Vanessa (p-value = 0.22). In the case of t_2 , statistically significant differences were observed in all cases.

3.1. Germination detection

As previously mentioned, the minimum value of $\eta_{2,0}$, referred to here by the time parameter of t_2 , corresponds to the observed onset of radicle growth, marking the beginning of the germination process. The following figure

(Fig. 6) shows the development of $\eta_{2,0}$ and grain length for two typical cases in the Tosca variety. In both cases, the $\eta_{2,0}$ minimum, and thus the onset of germination, occurs after approximately 30 h of hydration. Both images also illustrate that at time t_2 there is an increase in $\eta_{2,0}$ and in the rate of grain length growth (see also Fig. 4a, c). The actual elongation of the grains is subtle: in the first case (grain no. 48), there is an increase of only 0.3 mm over 10 hours following germination detection, while in the second case (grain no. 61), there is an increase of 0.6 mm. The time progression of both graphs suggests that grain elongation during hydration can be quite variable. In the first case, some acceleration in elongation is observed after 40 h of hydration, while in the second case, more uniform elongation is observed for times greater than t_2 .

Figure 7 contains images of the grains whose development was described in Fig. 6. Grain no. 48 (Tosca) is shown on the left (Fig. 7a, c), and grain no. 61 (Tosca) is presented on the right (Fig. 7b, d). The upper two images in the figure correspond to t_2 , marking the beginning of germination, while the images in the lower half relate to the moment 10 h after the start of germination. Germination begins when the radicle starts to penetrate the pericarp of the grain. However, this is not yet visible at time t_2 (the process is just beginning). In Fig. 7c, d, the difference between



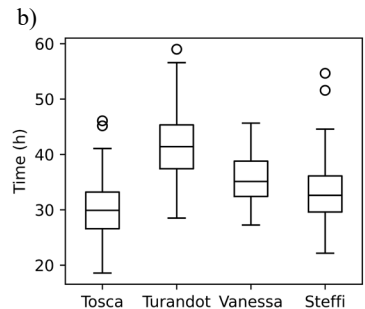
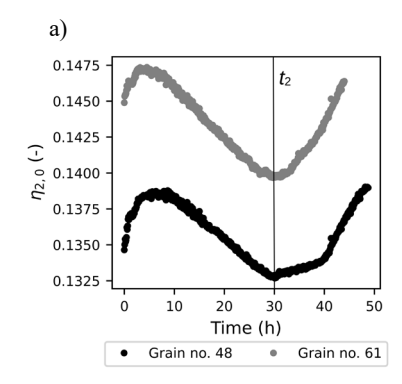


Fig. 5. Comparison of times t_1 (a) and t_2 (b) for the examined varieties. Median values, interquartile ranges, outside values, and outliers are depicted in the box plots. The times t_1 differ significantly among the analysed varieties, with no significant difference found only between Tosca and Vanessa (p-value = 0.22). The times t_2 are different for all varieties. The comparison was performed using the Kruskal-Wallis test followed by the Dunn test.



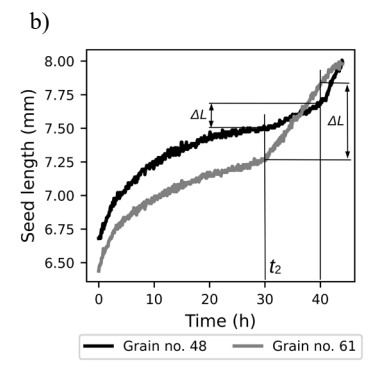


Fig. 6. Development of $\eta_{2,0}$ (a) and length (b) in two grains of the Tosca variety. Germination was detected in both images around the 30-hour mark. The graphs highlight the elongation of the grains over a 10-hour interval following the onset of germination (ΔL). In these cases, ΔL was found to be 0.3 mm and 0.6 mm for grains no. 48 and no. 61.

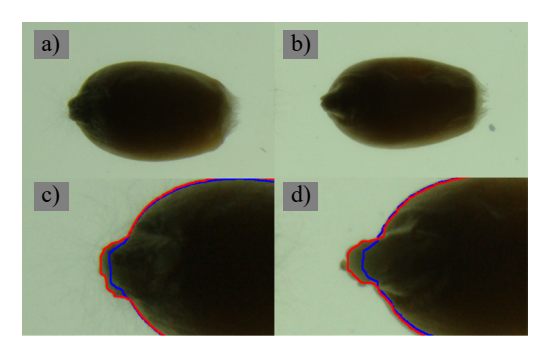


Fig. 7. Images of Tosca variety grains at time t_2 (a), (b) and details of the grains around the embryo at time $t_2 + 10$ h (c), (d). In parts (c) and (d), the outlines are colour-coded as detected at time t_2 (blue) and at $t_2 + 10$ h (red). These are the same grains as in Fig. 6, (a), (c) – grain no. 48, (b), (d) – grain no. 61.

times t_2 and $t_2 + 10$ h is highlighted in colour. The blue colour indicates the outlines of the grain at t_2 , while the red colour marks the state of the grain outlines at $t_2 + 10$ h. The images show that during this interval, the grain changed its shape mainly in the area of the embryo. The growth of the embryo is relatively small, making it challenging to detect any changes to this area even after 10 h of germination.

If we examine how germination detection is conducted in the systems used, we find that the detection software assumes a significant change in shape, size, or colour (Ducournau et al., 2004; Awty-Carroll et al., 2018; Joosen et al., 2010). If the radicle is not sufficiently developed, its direct detection cannot function in these cases, meaning that germination will be detected significantly later; the methods mentioned earlier in this study were designed to detect "visible germination". Our method is based on detecting shape changes in swelling grains at a high level of sensitivity. This allows us to detect germination very close to its onset.

3.2. Imbibition and germination parameters

Figure 8 shows a comparison for the individual varieties using box plots. The significance of the differences was also verified using the Kruskal-Wallis test followed by the Dunn test. In all cases, the Kruskal-Wallis test confirmed differences between the varieties (p-value < 1e-7), and in most cases, statistically significant differences between partial pairs were also confirmed with p-value < 0.05. Cases where the differences are not significant are summarised in Table 2.

The previously mentioned and discussed parameter t_{infl} represents the position of the inflection point located between the values t_1 and t_2 on the curve of $\eta_{2,0}$ as a function of time. The values of t_{infl} are typically in the range of 10 to 20 h. In the case of the Tosca and Vanessa varieties, t_{infl} is approximately at the midpoint of the germination process, while for Turandot and Steffi, t_{infl} was detected before the midpoint corresponding to the onset of germination. Notably, for the Turandot variety, although t_{infl} was detected

earlier than for the other varieties, this variety begins to germinate later than the others. The parameter t_{inft} is likely influenced by the details of the hydration mechanisms of the endosperm.

The increase in the area of grains during hydration is described by the parameters ΔA_1 , ΔA_{12} , and C_{1n} , which represent the relative increase compared to the initial area. In the first phase of germination (ΔA_1) , the area of the grains typically increases by approximately 5 to 15%. At the moment of germination, the total increase in area $(\Delta A_1 + \Delta A_{12})$ is around 20 to 30%. A significant increase in grain area was observed in the Tosca variety, which also germinated the fastest. The parameter C_{1n} represents the theoretical maximum increase in area over time starting from time t_1 and is derived from Eq. (4). Its values range approximately from 25 to 40%, which corresponds to about double the parameter ΔA_{12} . It is interesting to note how significantly this parameter differs among the studied varieties. This may be influenced, among other factors, by the different compositions of their endosperm.

The definition of $C_{ratio} = C_1 / (2 C_2 a_0)$ is also derived from Eq. (4) (Table 1). This parameter expresses the average rate of area growth of the grain from time t_1 to C_2 , where the increase in area corresponds to half of the maximum achievable increase. Table 1 also includes the parameter l_s , which uniquely describes the development of the grain after the onset of germination: it represents the rate of elongation of the grain over a period of 10 h of hydration starting from t_2 . Since the elongation of the grain is primarily influenced by the development of the seedling at this moment, it can be assumed that l_s corresponds to the vitality of the grain at the very onset of germination. The rate of elongation is relatively small, averaging between 0.02 and 0.04 mm h⁻¹.

The relationships between individual parameters were further examined using principal component analysis (PCA). Several parameters correlated with each other significantly, making this analysis appropriate. Only l_s showed few significant correlations and was therefore excluded from the analysis. The outputs of the principal component analysis are displayed in Fig. 9. Three components (PC1, PC2, and PC3) were identified for the data, which together explain 67.7% of the observed variability. The graphs in Fig. 9a and b indicate some differences among the varieties. These differences arise not only from the different initial parameters (a_0, η_0) and variations in the onset of germination but also, to a large extent, from parameters describing the imbibition process, which aligns with the work of Khan et al. (2024). The Vanessa and Turandot varieties appear to be the most distinct, with Vanessa showing particularly greater divergence from the others. The varieties primarily differ in the first component PC1, which accounts for the largest share of variability (34.2%).

In Figure 9c, d, the analysed parameters are displayed as vectors according to their contributions to the individual components. This allows for some inference about which

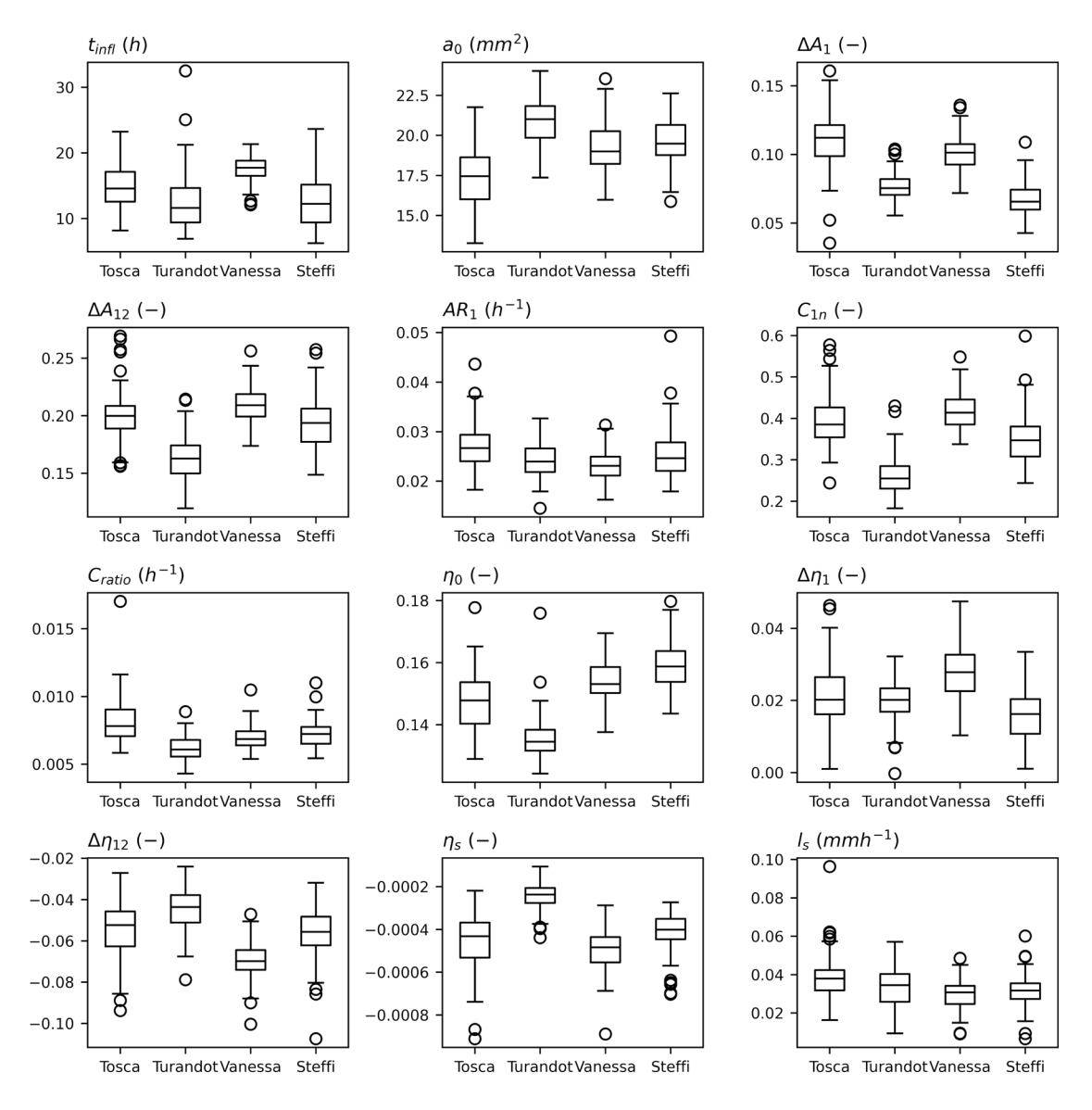


Fig. 8. Comparison of the parameters from Table 1 (excluding t_1 and t_2) among the varieties. Median values, interquartile range, outside values, and outliers are depicted in the box plots. The statistical significance of differences between the varieties was verified using the Kruskal-Wallis test, followed by the Dunn test (Table 2).

parameters represent the various components. PC1 is most influenced by η_S , which is related to the rate of shape change of the grain during germination. PC1 also partially represents the share of C_{1n} , ΔA_{12} , $\Delta \eta_{12}$, and a_0 . Except for a_0 , these parameters describe the change in the size and shape of the grain during the second phase of germination. This supports our previous findings that smaller grains exhibit faster imbibition during the second phase (Blahovec and Lahodová, 2015). PC2 is most influenced by t_1 , t_{infl} , AR_1 , and C_{ratio} . These parameters are largely associated with the dynamics of grain development. PC3 is primarily influenced by ΔA_1 and ΔA_{12} , which also have some effect on PC1.

3.3. Relationship between water uptake and germination parameters

The parameters t_2 and l_S provide information about the onset of germination and the vitality of the grain in the first ten hours after germination begins. The following table (Table 3) presents the correlations between the onset of germination t_2 and other parameters. Relatively significant positive correlations were found for the parameter ΔA_{12} . However, this relationship is logical and may not necessarily be directly related to the onset of germination. A seed that germinates later has time to absorb more water. Statistically significant correlations were found for parameters associated with the dynamics of wheat grain development, specifically ΔR_1 , C_{ratio} , and η_S . Since

Table 2. Results of the Dunn test for the parameters monitored in Fig. 8. The table includes only cases where no significant difference was found among the varieties. In cases not listed in the table, significant differences were observed among all varieties (p-value < 0.05)

Parameter	Variety pairings without significant differences	p-value		
t_{infl}	Turandot – Steffi	0.37		
a_0	Vanessa – Steffi	0.08		
ΔA_1	_	=		
ΔA_{12}	Tosca – Steffi	0.10		
AR_1	Turandot – Vanessa Turandot – Steffi	0.08 0.14		
C_{1n}	_	_		
C_{ratio}	Vanessa – Steffi	0.07		
η_0	_	_		
$\Delta \eta_1$	Tosca – Turandot	0.45		
$\Delta\eta_{12}$	Tosca – Steffi	0.45		
η_S	_	_		
l_S	Turandot – Steffi Vanessa – Steffi	0.11 0.27		

the dynamics of grain development relate to the ability of grains to absorb water (Miller *et al.*, 2018), these relationships could suggest that a faster water uptake facilitates earlier germination. A significant correlation was also found between the initial size and shape of the grains. According to our data, smaller and more elongated grains (with a higher $\eta_{2,0}$ value) germinate more quickly. Low values of correlation coefficients were found for the parameters ΔA_1 , $\Delta \eta_1$, C_{1n} , and l_s .

Table 4 presents the correlations of l_s with the other investigated parameters. This table contains only a small number of significant correlations. Tosca stands out among the varieties, as small but significant correlations were found within six parameters. However, this may also have been influenced by the larger sample size used for this variety.

The previous results suggest that the onset of grain germination in the studied varieties is influenced by certain parameters that can be determined prior to the actual detection of germination. Using backward stepwise regression (Longo-Minnolo *et al.*, 2024), a linear model was sought to predict the onset of germination. Parameters ΔA_{12} , $\Delta \eta_{12}$, and l_S were excluded in advance. None of these parameters can

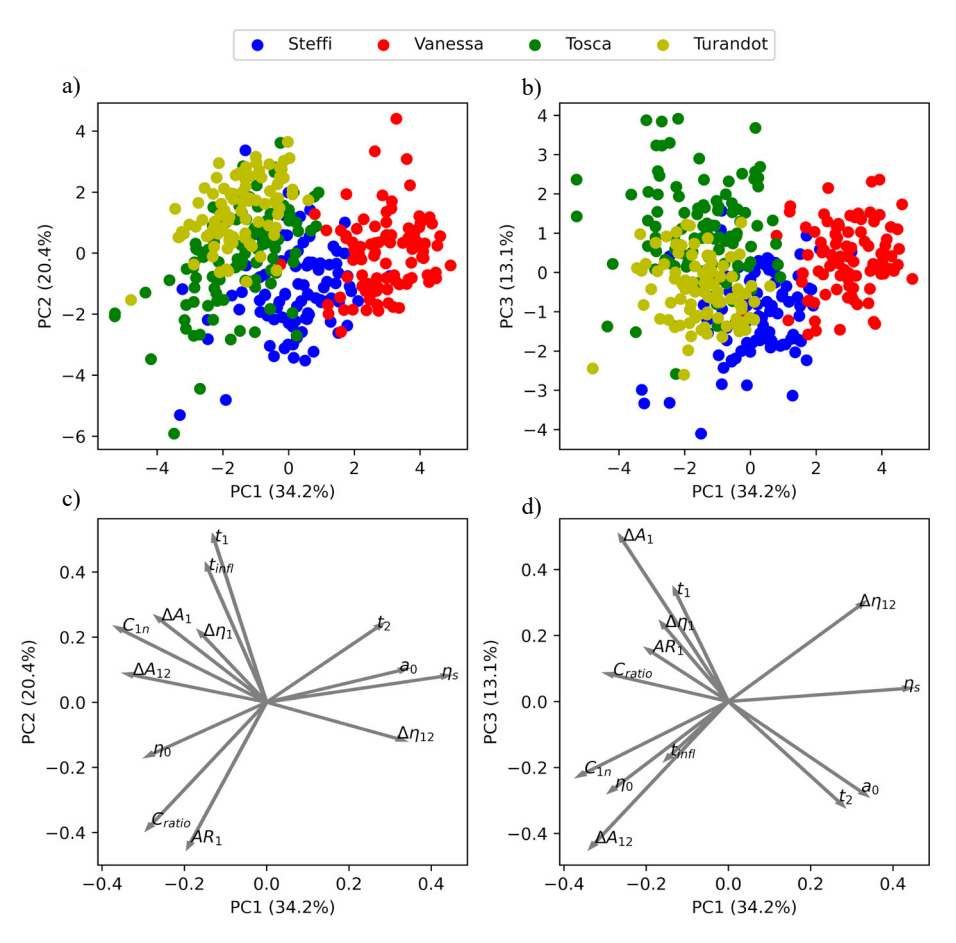


Fig. 9. Principal component analysis for the examined parameters: (a), (b) – plots of the principal components for PC1, PC2, and PC3; (c), (d) – loading plots for PC1, PC2, and PC3.

Table 3. Correlations of the investigated parameters with t_2 (time corresponding to the onset of germination), presenting the Pearson correlation coefficient for significant relationships (p-value < 0.05). Correlations greater than 0.5 are shown in bold

Variety	t_1	t_{infl}	a_0	ΔA_1	ΔA_{12}	AR_1	C_{1n}	C_{ratio}	η_0	$\Delta \eta_1$	$\Delta\eta_{12}$	η_S	l_S
Tosca	0.29	0.34	0.47	-	0.47	-0.51	-	-0.44	-0.23	_	-0.49	0.25	-0.22
Vanessa	_	_	0.33	_	0.28	-0.22	_	-	-0.28	-0.21	-0.24	0.24	0.22
Turandot	0.36	0.23	0.33	_	0.47	-0.41	_	-0.42	-0.47	_	_	0.54	_
Steffi	_	_	_	-0.21	0.58	_	_	-0.24	-0.29	_	-0.55	_	_

Table 4. Correlations of l_s with the other evaluated parameters (Pearson correlation coefficient). Only statistically significant values are presented with p-value>0.05

Variety	t_1	t_2	t_{infl}	A_0	ΔA_1	ΔA_{12}	AR_1	C_{1n}	C_{ratio}	η_0	$\Delta \eta_1$	$\Delta \eta_{12}$	η_S
Tosca	_	-0.22	-0.29	-0.32	-	_	0.32	_	0.25	-	_	_	-0.28
Vanessa	_	0.22	_	_	_	_	_	_	_	_	_	_	_
Turandot	_	_	_	_	_	_	_	_	_	_	_	_	_
Steffi	_	_	_	_	_	0.26	-	_	_	_	_	-0.26	_

be determined before the detection of germination, and the first two parameters (ΔA_{12} , $\Delta \eta_{12}$) even directly contain t_2 in their definitions. The dependent variable t_2 was left unnormalised, while the other parameters (independent variables) were normalised according to Eq. (5). During the calculation, the parameters t_{infl} and $\Delta \eta_1$ were gradually excluded because their contribution to the model was not statistically significant (p-value < 0.05). Although the model could be used to predict the onset of germination, its purpose in this article is primarily to demonstrate the relationship with the dynamics of imbibition.

The resulting coefficients of the model are presented in Table 5, and the relationship between the actual onset of germination and the predicted onset of germination is shown in Fig. 10. Different varieties are distinguished by colour. The figure also displays the graph's axis (black line), which represents the position of perfect prediction. While the model tends to add time during rapid germination, the behaviour is the opposite for delayed germination.

The correlation coefficients in Table 3, as well as the coefficients of the model in Table 5, indicate a relationship between the dynamics of imbibition and germination time. This is evident in the coefficients for AR_1 , C_{ratio} , and η_s . Both AR_1 and C_{ratio} express the rate of area growth, while η_s reflects the rate of shape change (the slope of the tangent to $\eta_{2,0}$ at the time t_{infl}). In all three cases, a faster development corresponds to earlier germination. Other parameters that correlate with the speed of germination are a_0 and η_0 , which represent the initial state of the grains. The analysis of the results shows that smaller and more elongated grains germinate more quickly. This could also relate to the dynamics of imbibition, as it can be assumed that smaller and more elongated grains will hydrate more rapidly. Our results also indicate that individual varieties can differ

Table 5. Coefficients of the linear model and their p-values. Multiple $r^2 = 0.5122$, adjusted $r^2 = 0.5017$, p-value < 2.2e-16. Standard error: 4.612 on 371 degrees of freedom. See also Fig. 10

Parameter	Value	p-value		
Intercept	34.9193	< 0.001		
t_1	3.3714	0.004		
a_0	1.7211	< 0.001		
ΔA_1	-4.0726	< 0.001		
AR_1	1.4809	0.042		
$oldsymbol{\eta}_0$	-2.1639	< 0.001		
η_S	-1.2230	0.006		
C_{1n}	-0.7822	0.012		
C_{ratio}	-2.1164	< 0.001		

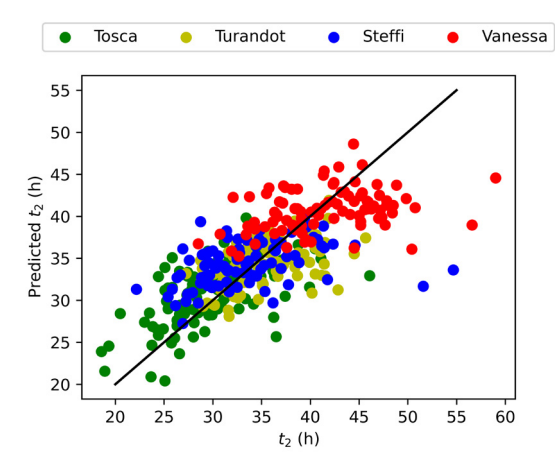


Fig. 10. Relationship between the actual onset of germination and the predicted onset of germination. Different varieties are distinguished by colour. The black line represents the axis of the graph, where exact predictions lie. The multiple r^2 value was 0.5122, and the adjusted r^2 value was 0.5017 (p-value < 2.2e-16). The standard error of the model was 4.612 h on 371 degrees of freedom. See also Table 5.

significantly from one another. For practical application, it would therefore be necessary to take into account the specific characteristics of individual varieties.

Some studies have been published on the relationship between the dynamics of imbibition and the rate of germination (e.g. Miller et al., 2018; Lechowska et al., 2019; Gómez-Maqueo et al., 2020). This relationship is not surprising, as grain hydration is a crucial condition for the initiation of processes that ultimately culminate in seedling development (Bewley, 1997). Gómez-Maqueo et al. (2020) propose the idea that the relative amount of water in a seed could serve as a universal marker for determining its biological state. However, in addition to the total water content, the current localisation of water is also crucial (Lewsey et al., 2025), particularly in the context of how a wheat grain gradually hydrates (Rathjen et al., 2009). The course of shape change and the parameters presented here (especially t_1) may therefore be highly useful for studying the biochemical processes occurring during imbibition, as the described shape transformation can provide an indication of when and to what extent endosperm hydration begins.

The dynamics of imbibition are closely linked to the issue of seed priming (Paparella $et\ al.$, 2015). Seed priming involves controlled imbibition, which is halted before the onset of the third phase of germination. Seeds prepared in this way may exhibit improved germination characteristics. In their experiments, Tanwar $et\ al.$ (2023) identified the optimal imbibition time for wheat priming to be approximately 12 h. According to our results, this duration is about two to three times longer than parameter t_1 and roughly corresponds to t_{inf} . The parameters we have introduced may therefore contribute to determining the optimal hydration period for different cultivars.

To date, there have been no publications attempting to predict the onset of germination based on the previous development of the grain during imbibition. One reason for this may be the inaccurately detected onset of germination. The linear model described here would not have been possible to construct without reliable detection of germination as close to the onset as possible. As already noted, commonly used methods are not capable of detecting germination at such an early stage as the method presented here (Ducournau *et al.*, 2004; Awty-Carroll *et al.*, 2018; Joosen *et al.*, 2010), since they are primarily designed to detect so-called visible germination. In other words, they require a relatively substantial change caused by the emerging radicle.

4. CONCLUSIONS

This article is based on the precise monitoring of the area, size, and shape of wheat grains during imbibition and germination. The shape development of individual grains (described by the image moment $\eta_{2,0}$) allows the process of imbibition and germination to be divided into three distinct

phases. In the first phase, designated here as t_1 , the grain's embryo is primarily hydrated; in the second phase, defined as the period between t_1 and t_2 , the endosperm is hydrated; and in the third phase, the radicle begins to grow (this stage could be referred to as actual germination). The grain does not behave as a homogeneous object, and for studying imbibition, it seems appropriate to consider the wheat grain as an object composed of at least two parts with different hydraulic properties.

Image moment development can be easily used to automatically detect and even analyse germination at a very early stage, much sooner than with other methods. The continued course of germination can be predicted already before the onset of radicle growth, at the end of imbibition, based on accumulated knowledge of the specific variety. This capability can not only expedite germination testing but may also be valuable for researching biochemical processes at the onset of germination.

The time at which the grains begin germinating is related to certain parameters that describe the dynamics of imbibition, as well as the shape and size of the grains. Using multiple regression, a model was created that can partially predict the onset of germination. The model's standard error was 4.612 h, and the coefficient of determination was 0.5017.

Declaration of interests: The authors declare that they have no known competing financial interests or personal relationships that could have appeared to influence the work reported in this paper.

Data availability: The dataset of our study can be obtained from the corresponding author upon reasonable request.

5. REFERENCES

Abenavoli, M.R., Cacco, G., Sorgonà, A., Marabottini, R., Paolacci, A.R., Ciaffi, M., Badiani, M., 2006. The inhibitory effects of coumarin on the germination of durum wheat (*Triticum turgidum* ssp. durum, cv. Simeto) Seeds. J. Chem. Ecol. 32, 489-506. https://doi.org/10.1007/s10886-005-9011-x

Al-Karaki, G.N., 1998. Response of wheat and barley during germination to seed osmopriming at different water potential.
J. Agronomy Crop Sci. 181, 229-235. https://doi.org/10.1111/j.1439-037X.1998.tb00422.x

ASABE Standards (2008) S358.2: Moisture Measurement-Forages. ASABE, St. Joseph., n.d.

Awty-Carroll, D., Clifton-Brown, J., Robson, P., 2018. Using k-NN to analyse images of diverse germination phenotypes and detect single seed germination in *Miscanthus sinensis*. Plant Methods 14, 5. https://doi.org/10.1186/s13007-018-0272-0

Bewley, J.D., 1997. Seed germination and dormancy. Plant Cell 1055-1066. https://doi.org/10.1105/tpc.9.7.1055

Blahovec, J., Lahodová, M., 2015. Moisture-induced changes of mass and dimension characteristics in some cereal grains. Int. Agrophys. 29, 1-12. https://doi.org/10.1515/intag-2015-0011

- Borisjuk, L., Rolletschek, H., Neuberger, T., 2012. Surveying the plant's world by magnetic resonance imaging. Plant J. 70, 129-146. https://doi.org/10.1111/j.1365-313X.2012.04927.x
- Colmer, J., O'Neill, C.M., Wells, R., Bostrom, A., Reynolds, D., Websdale, D., *et al.*, 2020. SeedGerm: a cost-effective phenotyping platform for automated seed imaging and machine-learning based phenotypic analysis of crop seed germination. New Phytologist 228, 778-793. https://doi.org/10.1111/nph.16736
- Dell' Aquila, A., 2009. Digital imaging information technology applied to seed germination testing. A review. Agron. Sustain. Dev. 29, 213-221. https://doi.org/10.1051/agro:2008039
- Dell'Aquila A., 2004. Application of a computer-aided image analysis system to evaluate seed germination under different environmental conditions. Italian J. Agronomy 8, 51-62.
- Diaz-Mendoza, M., Diaz, I., Martinez, M., 2019. Insights on the proteases involved in barley and wheat grain germination. IJMS 20, 2087. https://doi.org/10.3390/ijms20092087
- Ducournau, S., Feutry, A., Plainchault, P., Revollon, P., Vigouroux, B., Wagner, M.H., 2004. An image acquisition system for automated monitoring of the germination rate of sunflower seeds. Computers Electronics Agric. 44, 189-202. https://doi.org/10.1016/j.compag.2004.04.005
- Ghosh, P.K., Jayas, D.S., Gruwel, M.L.H., White, N.D.G., 2007. A magnetic resonance imaging study of wheat drying kinetics. Biosystems Eng. 97, 189-199. https://doi.org/10.1016/j.biosystemseng.2007.03.002
- Gómez-Maqueo, X., Soriano, D., Velázquez-Rosas, N., Alvarado-López, S., Jiménez-Durán, K., Garciadiego, M.D.M., et al., 2020. The seed water content as a time-independent physiological trait during germination in wild tree species such as Ceiba aesculifolia. Sci. Rep. 10, 10429. https://doi. org/10.1038/s41598-020-66759-3
- Gonzalez, R.C., Woods, R.E., 2007. Digital Image Processing, 3. ed. ed. Pearson/Prentice Hall, Upper Saddle River, NJ.
- Gruwel, M.L.H., Chatson, B., Yin, X.S., Abrams, S., 2001. A magnetic resonance study of water uptake in whole barley kernels. Int. J. Food Sci. Tech. 36, 161-168. https://doi.org/10.1046/j.1365-2621.2001.00445.x
- Halcro, K., McNabb, K., Lockinger, A., Socquet-Juglard, D., Bett, K.E., Noble, S.D., 2020. The BELT and phenoSEED platforms: shape and colour phenotyping of seed samples. Plant Methods 16, 49. https://doi.org/10.1186/ s13007-020-00591-8
- Joosen, R.V.L., Kodde, J., Willems, L.A.J., Ligterink, W., Van Der Plas, L.H.W., Hilhorst, H.W.M., 2010. GERMINATOR: a software package for high-throughput scoring and curve fitting of Arabidopsis seed germination: GERMINATOR software for Arabidopsis seed germination. Plant J. 62, 148-159. https://doi.org/10.1111/j.1365-313X.2009.04116.x
- Khan, T., Jamil, M., Ali, A., Rasheed, S., Irshad, A., Maqsood, M.F., et al., 2024. Exploring water-absorbing capacity: a digital image analysis of seeds from 120 wheat varieties. Sci. Rep. 14, 6757. https://doi.org/10.1038/s41598-024-57193-w
- Kikuchi, K., Koizumi, M., Ishida, N., Kano, H., 2006. Water uptake by dry beans observed by micro-magnetic resonance imaging. Annals Botany 98, 545-553. https://doi.org/10.1093/aob/mcl145

- Kornarzyński, K., Dziwulska-Hunek, A., Kornarzyńska-Gregorowicz, A., Sujak, A., 2018. Effect of electromagnetic stimulation of amaranth seeds of different initial moisture on the germination parameters and photosynthetic pigments content. Sci. Rep. 8, 14023. https://doi.org/10.1038/s41598-018-32305-5
- Kornarzyński, K., Pietruszewski, S., Łacek, R., 2002. Measurement of the water absorption rate in wheat grain. Int. Agrophysics 16, 33-36.
- Kroulík, M., Hůla, J., Rybka, A., Honzík, I., 2016. Pneumatic conveying characteristics of seeds in a vertical ascending airstream. Res. Agric. Eng. 62, 56-63. https://doi.org/10.17221/32/2014-RAE
- Lancelot, E., Bertrand, D., Hanafi, M., Jaillais, B., 2017. Near-infrared hyperspectral imaging for following imbibition of single wheat kernel sections. Vibrational Spectroscopy 92, 46-53. https://doi.org/10.1016/j.vibspec.2017.05.001
- Lechowska, K., Kubala, S., Wojtyla, Ł., Nowaczyk, G., Quinet, M., Lutts, S., Garnczarska, M., 2019. New insight on water status in germinating *Brassica napus* seeds in relation to priming-improved germination. IJMS 20, 540. https://doi.org/10.3390/ijms20030540
- Lev, J., Blahovec, J., 2017. Imbibition of wheat seeds: Application of image analysis. Int. Agrophys. 31, 475-481. https://doi.org/10.1515/intag-2016-0072
- Lev, J., Chalupa, B., Blahovec, J., 2017. Shape development of wheat seeds during germination. Presented at the 16th Int. Sci. Conf. Eng. Rural Develop. https://doi.org/10.22616/ ERDev2017.16.N267
- Lev, J., Kameneva, L., Blahovec, J., 2019. Detection of the entrance of Lugol's solution into the aleurone layer during germination. Int. Agrophys. 33, 383-388. https://doi.org/10.31545/intagr/110849
- Lewsey, M.G., Bassel, G.W., Whelan, J., 2025. Dynamic and spatial control of cellular activity dur-ing seed germination. Current Opinion in Plant Biology 86, 102754. https://doi.org/10.1016/j.pbi.2025.102754
- Loddo, A., Loddo, M., Di Ruberto, C., 2021. A novel deep learning based approach for seed image classification and retrieval. Computers Electronics Agric. 187, 106269. https://doi.org/10.1016/j.compag.2021.106269
- Longo-Minnolo, G., Consoli, S., Vanella, D., Pappalardo, S., Guarrera, S., Manetto, G., et al., 2024. Delineating citrus management zones using spatial interpolation and UAV-based multispectral approaches. Computers Electronics Agric. 222, 109098. https://doi.org/10.1016/j.compag.2024.109098
- Louf, J.-F., Zheng, Y., Kumar, A., Bohr, T., Gundlach, C., Harholt, J., *et al.*, 2018. Imbibition in plant seeds. Phys. Rev. E 98, 042403. https://doi.org/10.1103/PhysRevE.98.042403
- Manley, M., Du Toit, G., Geladi, P., 2011. Tracking diffusion of conditioning water in single wheat kernels of different hardnesses by near infrared hyperspectral imaging. Analytica Chimica Acta 686, 64-75. https://doi.org/10.1016/j. aca.2010.11.042
- Manz, B., Müller, K., Kucera, B., Volke, F., Leubner-Metzger, G., 2005. Water uptake and distribution in germinating tobacco seeds investigated in vivo by nuclear magnetic resonance imaging. Plant Physiol. 138, 1538-1551. https://doi. org/10.1104/pp.105.061663

- Mares, D.J., Mrva, K., 2014. Wheat grain preharvest sprouting and late maturity alpha-amylase. Planta 240, 1167-1178. https://doi.org/10.1007/s00425-014-2172-5
- Mebatsion, H.K., Paliwal, J., Jayas, D.S., 2012. Evaluation of variations in the shape of grain types using principal components analysis of the elliptic Fourier descriptors. Computers Electronics Agric. 80, 63-70. https://doi. org/10.1016/j.compag.2011.10.016
- Miller, N.D., Stelpflug, S.C., Kaeppler, S.M., Spalding, E.P., 2018. A machine vision platform for measuring imbibition of maize kernels: quantification of genetic effects and correlations with germination. Plant Methods 14, 115. https:// doi.org/10.1186/s13007-018-0383-7
- Moret-Fernández, D., Tormo, J., Latorre, B., 2024. A new methodology to characterize the kinetics of a seed during the imbibition process. Plant Soil 498, 181-197. https://doi.org/10.1007/s11104-023-06427-3
- Munz, E., Rolletschek, H., Oeltze-Jafra, S., Fuchs, J., Guendel, A., Neuberger, T., et al., 2017. A functional imaging study of germinating oilseed rape seed. New Phytologist 216, 1181-1190. https://doi.org/10.1111/nph.14736
- Nakanishi, T.M., Matsubayashi, M., 1997. Nondestructive water imaging by neutron beam analysis in living plants. J. Plant Physiol. 151, 442-445. https://doi.org/10.1016/ S0176-1617(97)80009-0
- Nehoshtan, Y., Carmon, E., Yaniv, O., Ayal, S., Rotem, O., 2021. Robust seed germination prediction using deep learning and RGB image data. Sci. Rep. 11, 22030. https://doi. org/10.1038/s41598-021-01712-6
- Nielsen, M.S., Damkjær, K.B., Feidenhans'l, R., 2017. Quantitative in-situ monitoring of germinating barley seeds using X-ray dark-field radiography. J. Food Eng. 198, 98-104. https://doi.org/10.1016/j.jfoodeng.2016.11.011
- Paparella, S., Araújo, S.S., Rossi, G., Wijayasinghe, M., Carbonera, D., Balestrazzi, A., 2015. Seed priming: state of the art and new perspectives. Plant Cell Rep. 34, 1281-1293. https://doi.org/10.1007/s00299-015-1784-y
- Rathjen, J.R., Strounina, E.V., Mares, D.J., 2009. Water movement into dormant and non-dormant wheat (*Triticum aestivum* L.) grains. J. Experimental Botany 60, 1619-1631. https://doi.org/10.1093/jxb/erp037

- Salanenka, Y.A., Taylor, A.G., 2011. Seedcoat permeability: uptake and post-germination transport of applied model tracer compounds. Horts 46, 622-626. https://doi.org/10.21273/HORTSCI.46.4.622
- Tanabata, T., Shibaya, T., Hori, K., Ebana, K., Yano, M., 2012.
 SmartGrain: high-throughput phenotyping software for measuring seed shape through image analysis. Plant Physiology 160, 1871-1880. https://doi.org/10.1104/pp.112.205120
- Tanwar, H., Mor, V.S., Sharma, S., Khan, M., Bhuker, A., Singh, V., et al., 2023. Optimization of 'on farm' hydropriming conditions in wheat: Soak-ing time and water volume have interactive effects on seed performance. PLoS ONE 18, e0280962. https://doi.org/10.1371/journal.pone.0280962
- Van As, H., Van Duynhoven, J., 2013. MRI of plants and foods. J. Magnetic Resonance 229, 25-34. https://doi.org/10.1016/j.jmr.2012.12.019
- Visscher, A.M., Castillo-Lorenzo, E., Toorop, P.E., Junio Da Silva, L., Yeo, M., Pritchard, H.W., 2020. Pseudophoenix ekmanii (*Arecaceae*) seeds at suboptimal temperature show reduced imbibition rates and enhanced expression of genes related to germination inhibition. Plant Biol. J. 22, 1041-1051. https://doi.org/10.1111/plb.13156
- Wiesnerová, D., Wiesner, I., 2008. Computer image analysis of seed shape and seed color for flax cultivar description. Computers Electronics Agric. 61, 126-135. https://doi.org/10.1016/j.compag.2007.10.001
- Wiwart, M., Moś, M., Wójtowicz, T., 2006. Studies on the imbibition of triticale kernels with a different degree of sprouting, using digital shape analysis. Plant Soil Environ. 52, 328-334. https://doi.org/10.17221/3449-PSE
- Zhao, J., He, Y., Li, X., Weng, X., Feng, D., Ying, J., *et al.*, 2020. An integrated RNA-Seq and physiological study reveals gene responses involving in the initial imbibition of seed germination in rice. Plant Growth Regul. 90, 249-263. https://doi.org/10.1007/s10725-019-00567-2
- Zhu, F., Paul, P., Hussain, W., Wallman, K., Dhatt, B.K., Sandhu, J., *et al.*, 2021. SeedExtractor: An open-source gui for seed image analysis. Front. Plant Sci. 11, 581546. https://doi.org/10.3389/fpls.2020.581546